

Article

Testing Joints between Walls Made of AAC Masonry Units

Radosław Jasiński ¹  and Iwona Galman ^{2,*} 

¹ Department of Building Structures, Silesian University of Technology, Akademicka 5, 44-100 Gliwice, Poland; radoslaw.jasinski@polsl.pl

² Department of Structural Engineering, Silesian University of Technology, Akademicka 5, 44-100 Gliwice, Poland

* Correspondence: iwona.galman@polsl.pl; Tel.: +48-32-237-22-88

Received: 15 December 2019; Accepted: 30 March 2020; Published: 2 April 2020



Abstract: Joints between walls are very important for structural analysis of each masonry building at the global and local level. This issue has often been neglected in the case of traditional joints and relatively squat walls. At present, the issue of wall joints is becoming particularly important due to the continuous drive for simplifying structures, introducing new technologies and materials. Eurocode 6 and other standards (American, Canadian, Chinese, and Japanese) recommend inspecting joints between walls, but no detailed procedures have been specified. This paper presents our own tests on joints between walls made of autoclaved aerated concrete (AAC) masonry units. Tests included reference models composed of two wall panels joined perpendicularly with a standard masonry bond (six models), with classic steel and modified connectors (twelve models). The shape and size of test models and the structure of a test stand were determined on the basis of the analysis of the current knowledge, pilot studies and numerical FEM (Finite Element Method) - based analyses. The analyses referred to the morphology and failure mechanism of models. Load-displacement relationships for different types of joints were compared and obtained results were related to results for reference models. The mechanisms of cracking and failure was found to vary, and clear differences in the behaviour and load capacity of each type of joint were observed. The individual working phases of joints were determined and defined, and an empirical approach was proposed for the determination of forces and displacement of wall joints.

Keywords: masonry structures; stiffening walls; wall joints; connectors; bed joint reinforcement

1. Introduction

The relationship between the type of bond between intersecting walls and the load-bearing capacity of test models was investigated by Castro et al. [1]. The models with no bond and with traditional masonry bond were tested. In the models without a bond, failure was caused by the loss of stability of a shorter wall component, while in the models with full bond, shearing along the whole height of the joint appeared. In addition to the joints constructed with masonry units, tests were also performed on reinforced joints. Paganoni and D'Ayala [2] investigated the effectiveness of steel anchors at the connections of intersecting walls. Similar tests were conducted by Maddaloni et al. [3,4]. However, in that case, investigations covered the effectiveness of innovative clamp anchors (rods made of carbon fibres wrapped longitudinally and spirally with a stainless steel mat). Unfortunately, there are only results from tests on connectors. Therefore, it is difficult to interpret their effectiveness because of the lack of any reference to the load-bearing capacity of joints made with a traditional masonry bond.

It is also worth mentioning tests performed by the authors in [5], in which pilot tests on masonry wall joints were presented. They were the first tests of that kind performed in Poland, and were among

the few that has been performed in Europe. Within this testing programme, three types of wall joints were compared: traditional masonry bonds, bonds with the use of steel L-shaped profiles and two-arm steel punched flat profiles. Traditional bonds exhibited almost five times higher load-bearing capacity than joints with steel L-profiles; the capacity of joints with flat profiles was almost twice higher.

The obtained test results encourage further investigations and continued work on the detailed description of joints and on the use of new methods for the construction of joints using other types of connectors, a higher number of connectors and the optimization of their shape. The performed pilot tests also demonstrated imperfections in test models and the testing method. Asymmetric failure images of two identical joints made it impossible to understand the work of a single joint. Despite the application of point forces close to the contact plane, cracks also occurred in the lower part of the web wall, which indicates bending of this part of the model and, consequently, complicates analyses. Another worrying phenomenon observed during the tests was the variation in deformations of steel connectors depending on the location of joints in relation to the loaded edge of the web wall, meaning the non-uniform work of the joints. Therefore, in further tests the authors decided to change the shape of test models and the method of load application.

The review of tests on joints described in [6] showed the lack of comprehensive studies on the behaviour of wall joints. That did not only refer to walls made of autoclaved aerated concrete (AAC) masonry units, but also made of other masonry units. A poor insight into the issue of joints and the mutual action of walls resulted in the neglect of calculations for such structures. Design standards lack guidelines for determining internal forces and stresses acting on wall intersections, and for determining conditions to verify the Ultimate Limit State (ULS) and the Serviceability Limit State (SLS). Those few tests are insufficient to describe the mechanism of joints work, much less to develop guidelines for their design and construction. Moreover, there is the need to design a connector in a new shape to satisfy the demands of the market, which is aimed at optimizing existing solutions. A new connector should meet requirements of ultimate states and simultaneously should have a simple construction, easy assembly and much higher performance reliability in the phase after reaching the greatest loading. Therefore, the overall aims of our own tests were specified and they included:

- Determination of the cracking and failure mechanisms of joints between AAC walls;
- Comparison of load capacity of wall joints using traditional masonry bonds and steel connectors;
- Optimization of the shape of a steel connector.

Moreover, the authors made an attempt to build simplified models representing the behaviour of reinforced and unreinforced joints, a process which was described in this paper and in [7]. Tests and analyses presented in this paper were completed with a new series of tests.

2. Programme of Our Own Tests

Three series (12 test models in total) with the same shape and dimensions were prepared and tested. T-shaped models were monosymmetric, with a web and flange length of ~89 cm. A vertical joint, whose structure varied intentionally, was formed between loaded and unloaded walls. A series of test models marked with **P** had traditional masonry joints between the web and the flange (Figure 1a). Those elements were regarded as reference models, whose mechanical parameters and behaviour at loading and failure were compared with results from other tests. In two other series, joints between webs and flanges were made with steel connectors (wall geometry acc. to Figure 1b). They were single punched flat profiles in series **B10** (Figure 1c), and modified flat profiles with a widened central part in series **BP10** (Figure 1d). This solution was proposed on the basis of our own tests [7] on perforated connectors. The widening of the central part was intended to increase the flexural capacity of the connector and its stiffness. The proposed shape is copyrighted via an application to the Polish Patent Office [8]. Joints made of galvanized perforated steel with a thickness of 1 mm were used in both series.

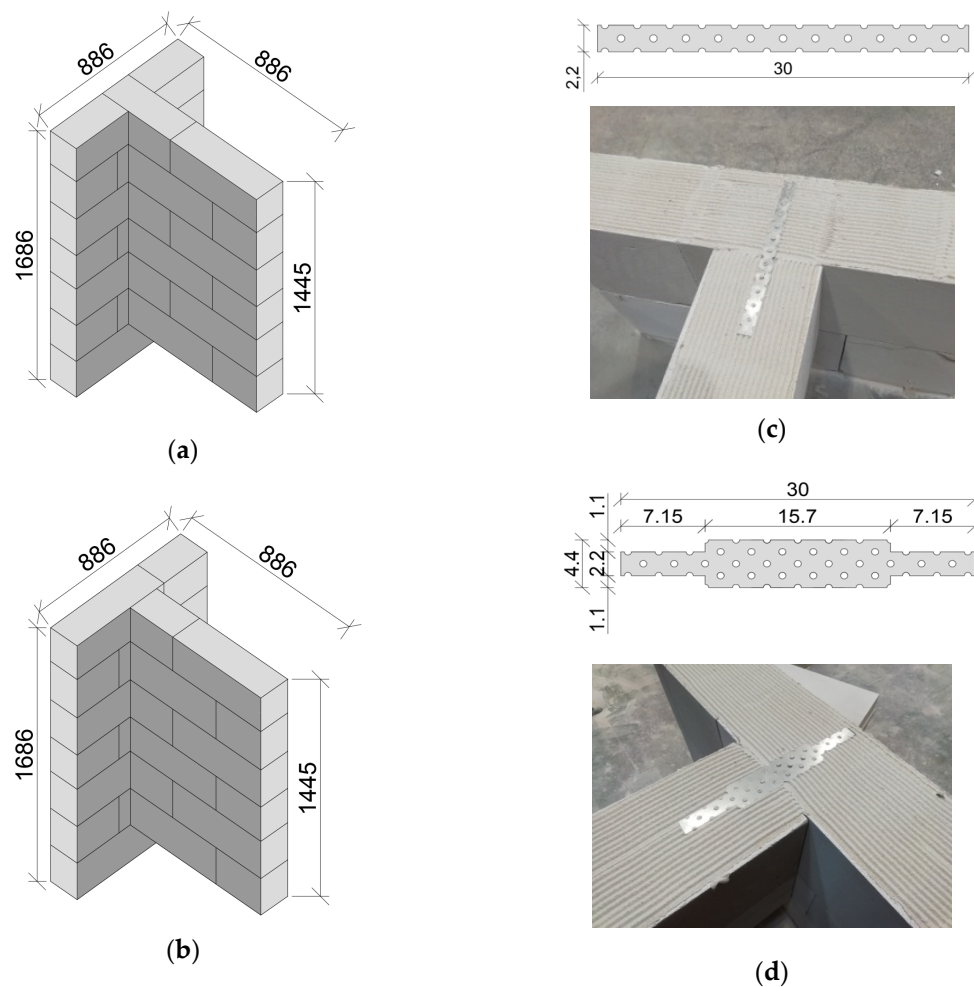


Figure 1. Geometry and details of test models and: (a) traditional masonry bond, P series, (b) walls with steel joints (B10 and BP10 series), (c) joining method with a punched flat bar, (d) joining method with a punched widened flat profile (mm).

Tests were conducted in a test stand specially designed for that purpose—see Figure 2. Models 1a and 1b with confining elements 3 and elements taking load 2 were put on the strong floor (panel 1b) and placed on a dynamometer 6, which with a resistor 4 acted as a fixed articulated support. Models were placed below a steel frame 8, to which a hydraulic actuator was fixed (with an operating capacity of 1000 kN), generating shearing at a constant displacement gain equal to 1 mm/min. The structure response was registered using an inductive force transducer with an operating capacity of 250 kN and reading accuracy of ± 2.5 kN. Prestress of 0.1 MPa was exerted using reinforced concrete elements 3 and steel strands 7 to model the considerable length of a joined wall in panel 1b. Models were loaded in one cycle until failure. Vertical load generating shear was transmitted linearly along the whole height of the wall through elements 2. As a result, shear stresses on joints were distributed uniformly. The loading and displacement of a loaded wall against the unloaded one were continually registered during tests. Two independent types of software were used to register data. One side of the test model was monitored using ARAMIS—an optical sensor of displacements. Another side was monitored with inductive transducers of displacement of type PJX-10, with an operating capacity of 10 mm and an accuracy of ± 0.002 mm.

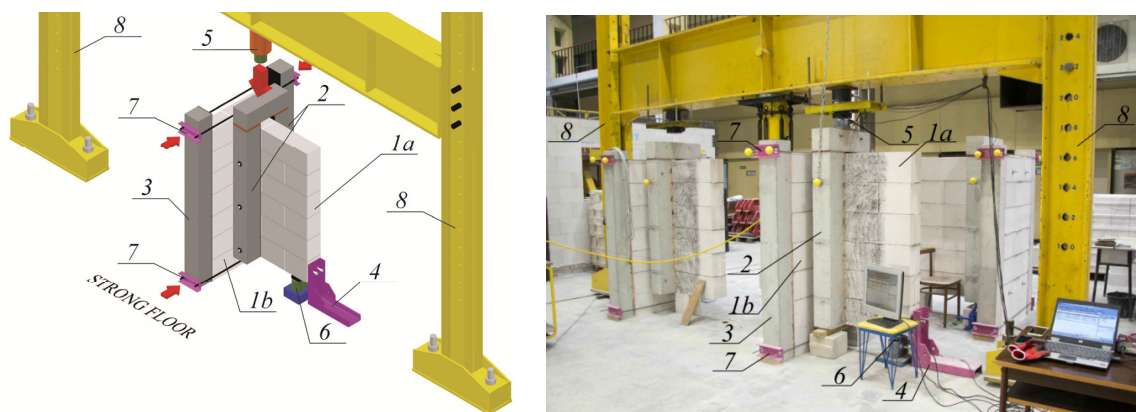


Figure 2. A scheme and photo of the test stand (longitudinal wall (1a), transverse wall (1b), reinforced concrete column transferring shear load (2), reinforced concrete pillars limiting horizontal deformation (3), horizontal support (4), system of the hydraulic cylinder and the force gauge used to induce shear stress (5), force gauge, vertical reaction (6), horizontal tie (7), steel frame (8)).

Tests were performed on models made of AAC masonry units with system mortar M5 class for the thin joints and the unfilled head joint. The compressive strength of the masonry specified in the code PN-EN 1052-1:2000 [9] and presented in [10] was $f_c = 2.97 \text{ N/mm}^2$, and the modulus of elasticity was $E_m = 2040 \text{ N/mm}^2$. The initial shear value determined according to the code PN-EN 1052-3:2004 [11] and presented in [12] was $f_{vo} = 0.31 \text{ N/mm}^2$.

The mean friction coefficient in joints without mortar was $\mu = 0.92$ [13]. The shear modulus determined according to the code ASTM E519-81 [14] and presented in [15] was $G = 329 \text{ N/mm}^2$. Mortar for thin joints was used in the tested elements for the AAC blocks. This mortar is dedicated to the erection of AAC masonry walls. Additional tests on steel connectors—see Figure 3—were conducted according to the standard [16]. Three elements were chosen randomly from each series of connectors and placed in the jaws of a testing machine. The basic mechanical parameters of the connectors were determined by controlling the displacement gain. The measurement of strains was non-contact with a video extensometer MEVIX 200. Strain was measured using a base with the length $L_e = 53.5 \text{ mm}$ in standard connectors and $L_e = 75.0 \text{ mm}$ in thickened connectors. Figure 3 illustrates (stress σ –strain ϵ) relationships. The stress–strain relationship of tested connectors was found to have no clear yield point. Therefore, results were approximated with a bi-linear relationship. A theoretical yield point f_y was determined at the intersection of straight lines. The slope of the tangent straight line presented within the range of 0 – f_y was assumed as the mean initial modulus of elasticity E_s . Tensile strength was determined at failure of specimens, and the tangent of the straight-line slope within the range of f_y – f_t was determined as the mean secant modulus of elasticity E_t . Test results for connectors and the research programme are compared in Table 1.

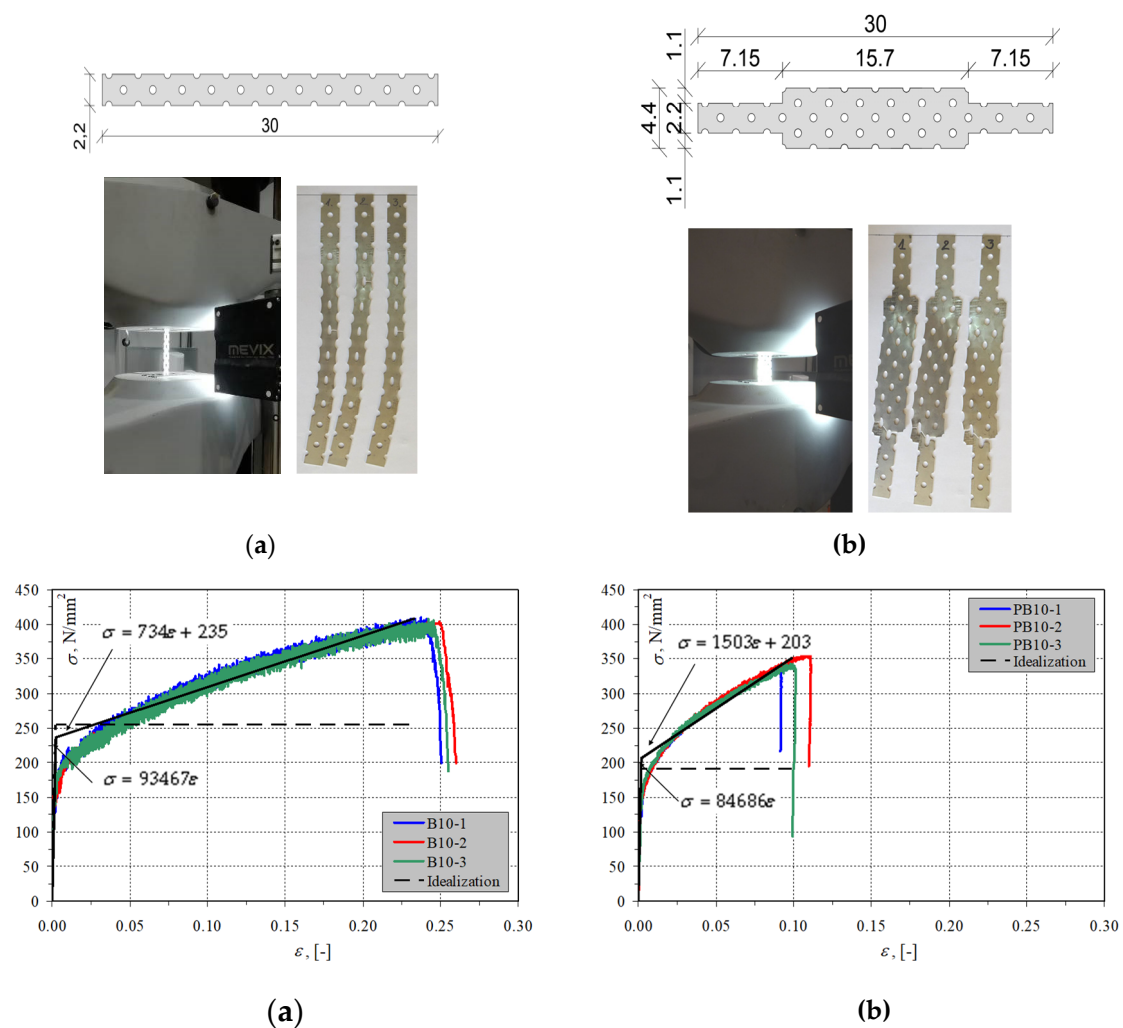




Figure 3. Test tested connectors: (a) connectors B10, (b) connectors BP10.

Table 1. Programme of tests and basic characteristics of connectors.

| Name of Series | Type of Joint | A mm ² | I mm ⁴ | f_y/f_t N/mm ² | E_s/E_t N/mm ² | Number of Models |
|----------------|--|----------------------|----------------------|--------------------------------|--------------------------------|------------------|
| P | Traditional masonry bond | – | – | – | – | 6 |
| B10 | Punched steel flat profile $B \times t = 22 \times 1$ mm  | 22 | 1.83 | 236/408 | 93467/743 | 3 |
| BP10 | Punched widened flat profile $B \times t = 44 \times 1$ mm  | 44 | 3.67 | 207/345 | 84686/1503 | 3 |

Area of gross section (A), moment of inertia of gross section (I), mean yield stress (f_y), tensile strength (f_t), mean initial modulus of elasticity (E_s), mean secant modulus of elasticity (E_t).

3. Test results and Analysis

3.1. Unreinforced Models

The behaviour of all unreinforced models was similar. No cracking noise and no visible splitting on the lateral surfaces of elements were noticed in the initial phase of loading. Non-dilatation strain in some parts of the wall was observed. That phase lasted until the appearance of the first diagonal cracks

in the adjacent vicinity of wall joints—see Figure 4a,b. Load increments caused the distinct development of cracks present at the location of joints and propagation towards the reinforced concrete column which transferred loading (Figure 4c). The greatest force was registered in that phase. Continued loading led to the distinct growth of mutual displacements and the rotation of joined walls. The joint was removed after failure—see Figure 4d. Almost vertical shearing of elements forming the bond was found. No clear damage was reported in the case of other elements.

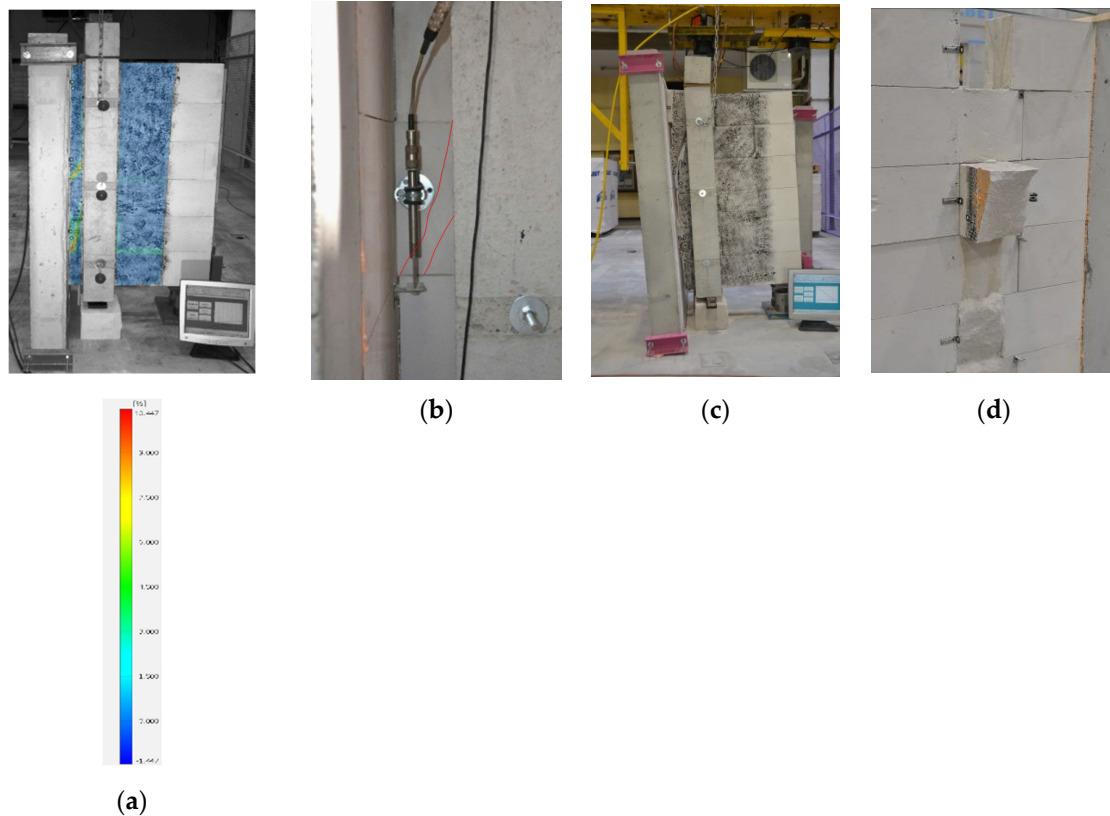


Figure 4. Destruction of models of series P (a) a first crack on the reference model P_2, (b) a first crack on the reference model P_6, (c) joint after failure P_5, (d) joint after failure P_3.

The cracking mechanism for elements is also visible on diagrams illustrating the relationship between the load N and relative (mutual) displacement u of bonded walls—see Figure 5. Until cracking of the contact surface observed under the load $N_{cr} = 27.3\text{--}54.1$ kN, increments in relative displacements u were almost directly proportional, and thus the working phase of the joint was called the elastic phase. After cracking in the post-elastic phase, stiffness was reduced. However, joints still had the capacity to take the load.

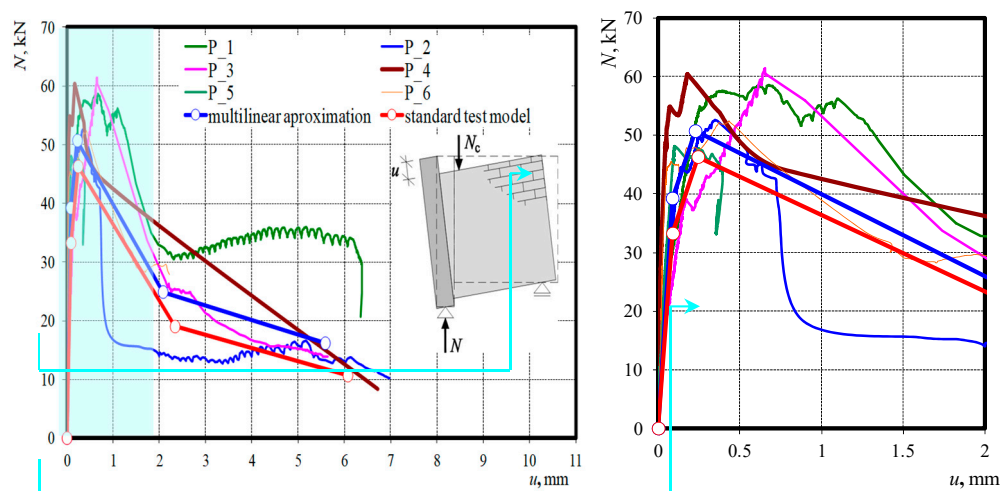


Figure 5. Relationship between the total force and mean displacement for test results and calculations.

This phase was completed at maximum force values within the range $N_u = 38.6\text{--}59.8$ kN. Continued attempts at loading in the failure phase resulted in a clear drop in the values of forces registered by a dynamometer, and an increment in relative displacements. Force was close to zero, and the joint had the capacity to take some load. In this phase, forces were called aggregate interlocking forces with values of $N_{ag} = 14.1\text{--}31.1$ kN. Further increment in joint displacements caused a minor load increase and hardening. The last registered forces, called residual forces, preceded the failure that resulted in the total splitting of bonded elements and their mutual rotation. Their value ranges were $N_r = 8.4\text{--}42.9$ kN. Forces and corresponding displacements are presented in Tables 2 and 3, and the linear approximation of results is shown in Figure 6. Joint stiffness was determined in each phase according to Equations (1)–(3) and they are presented in Table 4:

Table 2. Test results for joints between unreinforced walls.

| Model | Force at the Time of Cracking | | Maximum Force | | Aggregate Interlocking Force | | Residual Force | |
|-------|-------------------------------|-------------------|-----------------|------------------|------------------------------|---------------------|-----------------|------------------|
| | $N_{cr,i}$ kN | $N_{cr,mv}$ kN | $N_{u,i}$ kN | $N_{u,mv}$ kN | N_{ag} kN | $N_{ag,mv,i}$ kN | $N_{r,i}$ kN | $N_{r,mv}$ kN |
| P_1 | 27.3 | 39.2 | 56.3 | 50.7 | 31.1 | 24.9 | 20.7 | 16.2 |
| P_2 | 42.6 | | 50.0 | | 14.7 | | 10.2 | |
| P_3 | 31.2 | | 38.6 | | 25.5 | | 13.8 | |
| P_4 | 54.1 | | 59.8 | | — | | 8.36 | |
| P_5 | 35.1 | | 48.1 | | — | | — | |
| P_6 | 45.1 | | 51.6 | | 28.264 | | 27.9 | |

Table 3. Test results for joints between unreinforced walls (displacements).

| Model | Displacement at the Time of Cracking | | Displacement Right before Failure | | Displacement at Aggregate Interlocking Force | | Residual Displacement | |
|-------|--------------------------------------|-------------------|-----------------------------------|------------------|--|-------------------|-----------------------|------------------|
| | $u_{cr,i}$ mm | $u_{cr,mv}$ mm | $u_{u,i}$ mm | $u_{u,mv}$ mm | $u_{ag,i}$ mm | $u_{ag,mv}$ mm | $u_{r,i}$ mm | $u_{r,mv}$ mm |
| P_1 | 0.07 | 0.09 | 0.31 | 0.23 | 2.43 | 2.08 | 6.36 | 5.58 |
| P_2 | 0.12 | | 0.25 | | 1.95 | | 6.97 | |
| P_3 | 0.12 | | 0.16 | | 2.22 | | 5.64 | |
| P_4 | 0.07 | | 0.17 | | – | | 6.72 | |
| P_5 | 0.06 | | 0.10 | | – | | – | |
| P_6 | 0.08 | | 0.36 | | 1.71 | | 2.22 | |

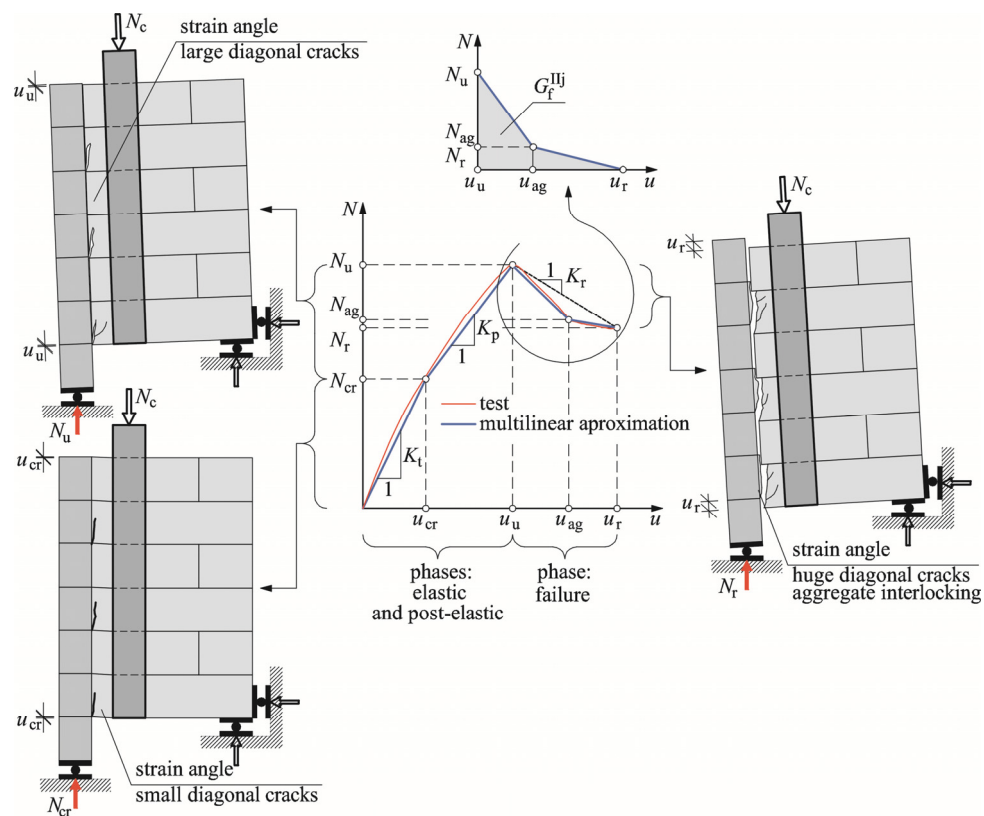
**Figure 6.** Approximation of work of unreinforced joints between masonry walls.

Table 4. Test results for joints between unreinforced walls (joint stiffness).

| Model | Elastic Joint Stiffness | | Post-Elastic Joint Stiffness | | Residual Joint Stiffness | |
|-------|-------------------------|--------------------|------------------------------|--------------------|--------------------------|--------------------|
| | $K_{t,i}$ MN/m | $K_{t,mv}$ MN/m | $K_{p,i}$ MN/m | $K_{p,mv}$ MN/m | $K_{r,i}$ MN/m | $K_{r,mv}$ MN/m |
| P_1 | 413 | 496 | 119 | 123 | 5.89 | 7.39 |
| P_2 | 341 | | 60 | | 5.93 | |
| P_3 | 268 | | 163 | | 4.51 | |
| P_4 | 804 | | 52.8 | | 7.86 | |
| P_5 | 562 | | 322 | | – | |
| P_6 | 590 | | 23 | | 12.75 | |

Joint stiffness in the elastic phase,

$$K_t = \frac{N_{cr}}{u_{cr}}, \quad (1)$$

joint stiffness in the post-elastic phase,

$$K_p = \frac{N_u - N_{cr}}{u_u - u_{cr}}, \quad (2)$$

joint stiffness in the failure phase,

$$K_r = \frac{|N_r - N_u|}{u_r - u_u}. \quad (3)$$

Validation of the Model with Unreinforced Wall Joints

Performed tests were used to generalize the obtained results by proposing the so-called standard model [17]. The following assumptions were made:

- A non-linear relationship $N-u$ determined from tests could be replaced with a multi-linear relationship expressing all observed phases:
 - The elastic phase observed in the load range $0-N_{cr}$;
 - The post-elastic phase observed in the load range $N_{cr}-N_u$;
 - The failure phase observed in the load range $N_u-N_{ag}-N_r$.
- It was suggested that all material parameters used in the model should be specified using standard and normalised methods;
- The model would be subjected to statistical validation on the basis of performed tests.

The following empirical relationships were recommended to determine forces and displacements in particular phases:

Forces and displacements in the elastic phase:

$$N_{cr} = \alpha_1 \tau_{cr,RL} A, \quad (4)$$

$$u_{cr} = N_{cr} / K_t = N_{cr} / \alpha K_{RL}. \quad (5)$$

Forces and displacements in the post-elastic phase:

$$N_u = \beta_1 \tau_{u,RL} A, \quad (6)$$

$$u_u = u_{cr} + (N_u - N_{cr}) / K_p = u_{cr} + (N_u - N_{cr}) / \beta K_t, \quad (7)$$

where $A = 0.26 \text{ m}^2$ is the joint area and α , α_1 , β and β_1 are empirical coefficients.

Shear parameters determined during tests on diagonal compression performed in compliance with ASTM E519-81 were $\tau_{cr,RL} = 0.192$ MPa, $\tau_{u,RL} = 0.196$ N/mm² and stiffness $K_{RL} = 117.1$ MN/m were used as reference values in above equations. At the beginning of the failure phase, residual and aggregate interlocking forces were determined from the following equations:

$$N_r = \gamma \tau_{u,RL} A, \quad (8)$$

$$N_{ag} = \gamma_1 \tau_{u,RL} A, \quad (9)$$

where γ and γ_1 are empirical coefficients.

Displacements corresponding to the aggregate interlocking force were determined from the following empirical relationship:

$$u_{ag} = \omega \tau_{u,RL} / K_{RL}, \quad (10)$$

where ω is the empirical coefficient.

Values of empirical coefficients were calculated using the results from material tests and tests on individual elements. Furthermore, boundary values of mean coefficients α , α_1 , β , β_1 , γ , γ_1 and ω were determined at the significance level $\alpha = 0.8$ to create the reference model [18]. As the sample size was small $n < 30$, the following relationship was used:

$$P\left(\bar{x} - t_{1-\alpha/2} \frac{S}{\sqrt{n}} < m < \bar{x} + t_{1-\alpha/2} \frac{S}{\sqrt{n}}\right) = 1 - \alpha, \quad (11)$$

where: $\bar{x} = \sqrt{\sum (x - \bar{x})^2 / n}$ is the mean value of the random sample, $S = \sqrt{\sum (x - \bar{x})^2 / (n - 1)}$ is the standard deviation of the sample, $t_{1-\alpha/2}$ are statistics with Student's t-distribution and $n-1$ degrees of freedom.

Lower and upper values from the confidence interval of mean coefficients are presented in Table 5.

Table 5. Validation of empirical coefficient of the model with unreinforced wall joints.

| Model | x_i | | | | | | |
|---|-------------------------------------|-------------------------------------|--|---|--|---|--|
| | $\alpha_i = \frac{K_{t,i}}{K_{RL}}$ | $\beta_i = \frac{K_{p,i}}{K_{t,i}}$ | $\alpha_{1,i} = \frac{N_{cr,i}}{\tau_{cr,RL} A}$ | $\beta_{1,i} = \frac{N_{u,i}}{\tau_{u,RL} A}$ | $\gamma_i = \frac{N_{r,i}}{\tau_{u,RL} A}$ | $\gamma_{1,i} = \frac{N_{ag,i}}{\tau_{u,RL} A}$ | $\omega_i = \frac{u_{ag,i} K_{RL}}{\tau_{u,RL} A}$ |
| P_1 | 3.51 | 0.29 | 0.55 | 1.10 | 0.4 | 0.6 | 5.61 |
| P_2 | 2.90 | 0.17 | 0.85 | 0.98 | 0.2 | 0.3 | 4.49 |
| P_3 | 2.27 | 0.61 | 0.62 | 0.76 | 0.3 | 0.5 | 5.13 |
| P_4 | 6.83 | 0.07 | 1.08 | 1.17 | 0.2 | – | – |
| P_5 | 4.78 | 0.57 | 0.70 | 0.94 | – | – | – |
| P_6 | 5.01 | 0.04 | 0.90 | 1.01 | 0.5 | 0.6 | 3.94 |
| n | 6 | 6 | 6 | 6 | 5 | 4 | 4 |
| \bar{x} | 4.22 | 0.29 | 0.79 | 0.99 | 0.32 | 0.49 | 4.80 |
| S | 1.7 | 0.2 | 0.2 | 0.1 | 0.2 | 0.1 | 0.7 |
| $t_{1-\alpha/2}$ | 1.48 | 1.48 | 1.48 | 1.48 | 1.53 | 1.64 | 1.64 |
| $\bar{x} - t_{1-\alpha/2} \frac{S}{\sqrt{n}}$ | 3.22 | 0.14 | 0.67 | 0.91 | 0.21 | 0.37 | 4.20 |
| $\bar{x} + t_{1-\alpha/2} \frac{S}{\sqrt{n}}$ | 5.22 | 0.44 | 0.91 | 1.08 | 0.43 | 0.60 | 5.39 |

In the failure phase, during which dry shear fracture of separating walls was observed, the joint behaviour was mapped on the basis of standard behaviours specified in PN-EN 1052-3:2004. Those tests included measurements of relative displacements of two masonry units joined with mortar and determination of fracture energy of the joint $G_f^{II} = 2.37 \times 10^{-4}$ MN/m [13], which could be used to describe the behaviour of the brittle material in the failure phase in accordance with the continuum

fracture mechanism. The failure phase was described on the basis of observations using two sections with forces varying from N_u to N_{ag} , and then from N_{ag} to N_r at corresponding displacements u_u , u_{ag} and u_r . Assuming that fracture energy per joint area G_f^{IIj} (expressed as the area below the diagram shown in Figure 6) was equal to fracture energy G_f^{II} , obtained from standard tests, the displacement corresponding to the residual force u_r was determined from the relationship:

$$\begin{aligned} AG_f^{II} = AG_f^{IIj} &= \frac{1}{2}(N_u - N_{ad})(u_{ad} - u_u) + (N_{ad} - N_r)(u_{ad} - u_u) \\ &+ \frac{1}{2}(N_{ad} - N_r)(u_r - u_{ad}) \\ \Rightarrow u_r &= \frac{2G_f^{II}A - N_u(u_{ag} - u_u) + N_{ag}u_u + N_r(u_{ag} - 2u_u)}{(N_{ag} - N_r)}. \end{aligned} \quad (12)$$

Following that procedure, two values defining the lower and upper limits of yjr confidence intervals matched each of the seven coefficients (Table 5). Maximum and minimum values of displacement expressed by the relationship in (12) depended on the previously used values and could be considered as independent variables. Thus, there were $\binom{7}{2}$ different combinations (without any repetitions) for coefficients. The minimum value of the mean square error calculated separately for forces and displacements was applied as a selection criterion. Optimal values of those coefficients were calculated from 21 combinations. A Mean Percentage of Error (MPE) was calculated [19] $MPE = \frac{1}{N} \sum_{N=1}^5 \frac{x_{obs} - x_{cal}}{x_{obs}}$. The minimum MPEs for calculated forces and displacements with respect to the coefficients listed in shaded cells in Table 5 were 16% (for force) and -6% (for displacement).

As a result, empirical relationships based on the results from model and standard tests, describing the work of joints in particular phases, are presented in Table 6, and calculated values and empirically obtained values are compared in Table 7 and Figure 5.

Table 6. Relationships describing the work of unreinforced joints between walls.

| Joint Phase | Force | Stiffness | Displacement |
|--------------------|-----------------------------|---------------------------------|--|
| Elastic phase | $N_{cr} = 0.67\tau_{u,RL}A$ | $K_t = 3.22K_{RL}$ | $u_{cr} = N_{cr}/3.22K_{RL}$ |
| Post-elastic phase | $N_u = 0.91\tau_{u,RL}A$ | $K_p = 0.14K_{RL}$ | $u_u = (N_u - N_{cr})/0.14K_{RL}$ |
| Failure phase | $N_{ag} = 0.37\tau_{u,RL}A$ | $(N_u - N_{ag})/(u_u - u_{ag})$ | $u_{ag} = 5.39\tau_{u,RL}A/K_{RL}$ |
| | $N_r = 0.21\tau_{u,RL}A$ | $K_r = (N_u - N_r)/(u_r - u_u)$ | $u_r = \frac{2G_f^{II}A - N_u(u_{ag} - u_u) + N_{ag}u_u + N_r(u_{ag} - 2u_u)}{(N_{ag} - N_r)}$ |

Table 7. Compared test results and our own calculations for the standard model.

| Test Results for | | | | Calculated Results for | | | |
|-------------------|------------------|-------------------|------------------|------------------------|-------------------|--------------------|-------------------|
| Forces | | | | Forces | | | |
| $N_{cr,mv}$ kN | $N_{u,mv}$ kN | $N_{ag,mv}$ kN | $N_{r,mv}$ kN | $N_{cr,cal}$ kN | $N_{u,cal}$ kN | $N_{ag,cal}$ kN | $N_{r,cal}$ kN |
| 39.2 | 50.7 | 24.9 | 16.2 | 33.3 | 46.3 | 19.0 | 10.7 |
| Displacements | | | | Displacements | | | |
| $u_{cr,mv}$ mm | $u_{u,mv}$ mm | $u_{ag,mv}$ mm | $u_{r,mv}$ mm | $u_{cr,cal}$ mm | $u_{u,cal}$ mm | $u_{ag,cal}$ mm | $u_{r,cal}$ mm |
| 0.09 | 0.243 | 2.08 | 5.58 | 0.09 | 0.24 | 2.34 | 6.53 |

Following the assumptions, calculated forces determining coordinates for particular phases of joint work were smaller than those obtained from tests, which was consistent with the assumptions. Considering the force causing cracks, the difference was 15%, and for the failure force, it was −9%. The biggest differences were found in the failure phase. Then, the calculated values N_{ag} and N_r were lower by 36% and 44% than mean empirical values. For relative displacement in the elastic phase, the calculated displacement differed from the average empirical value by only 3%, and by 7% in case of the greatest force. In the failure phase, displacements corresponding to forces N_{ag} and N_r differed by 12% and 17%, respectively. The delivered results were sufficient to predict forces with satisfactory accuracy and thus to verify properly the SLS conditions for joints. Greater differences were found for displacements, which are crucial for verifying SLS conditions. The biggest discrepancy was obtained for the maximum load.

3.2. Reinforced Models

In the models of series **B10** and **BP10**, reinforced with steel connectors, no cracks on walls typical for unreinforced models were observed for the whole range of loading. Displacements of interconnected wall panels were unnoticeable in the initial phase of loading. At a given moment, a rapid increase in displacements was clearly visible to the naked eye. However, it was still possible to continue the loading of the models until the moment of failure. Failure was rapid and caused shearing of the joint and a distinct vertical displacement (by ca. 17 mm) of the wall web—see Figure 7b. The wall settled on the wooden protection. Models at the point of failure are shown in Figure 7a. The failure of the models of series **B10** and **BP10** was caused by the yielding and bending of steel flat profiles in the vicinity of the contact surface (Figure 7c,d). Spalling of masonry units beneath each connector was observed at the wall edge (see arrows in Figure 7c,d). The measured length of spalling areas was ca. 15 mm. However, no shear fracture of the connector was observed in the mortar laid in bed joints due to the holes in the flat profile. Mortar penetrating through the holes was not subjected to shearing. It acted as a dowel and prevented displacement. For **B10** models, an increase in displacements was observed at lower values of the loading force when compared to **BP10** models.

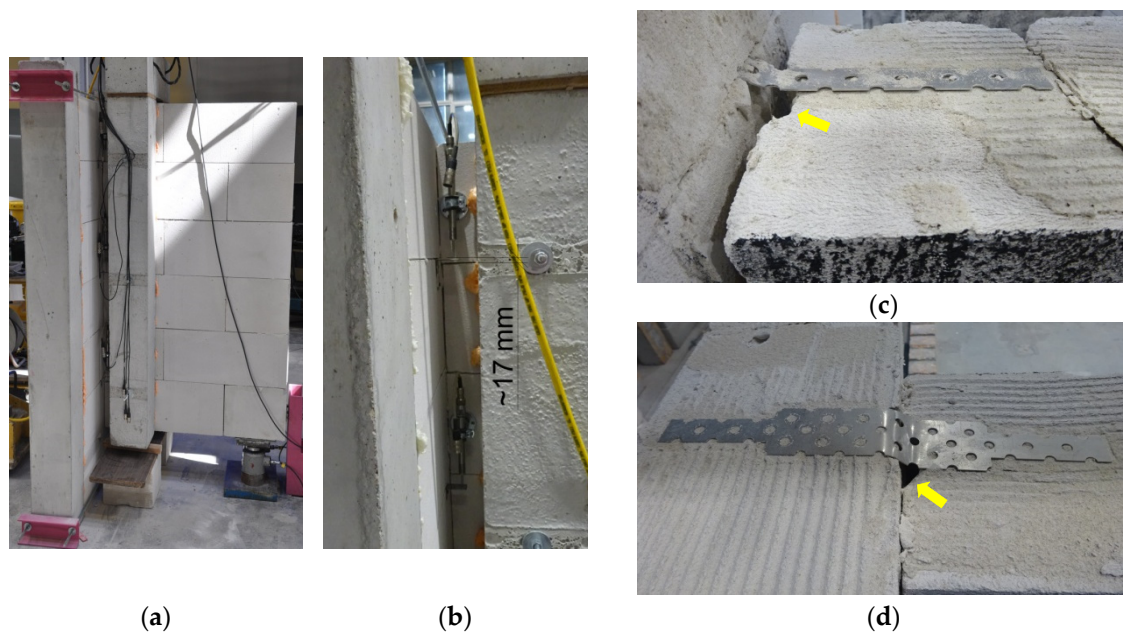


Figure 7. Failure of reinforced models: (a) damaged model (B10_1), (b) damaged model with dimensioned displacement between bed joints (B10_2), (c) typical bending of punched flat profile near the contact surface (B10_1), (d) typical bending of punched flat profile near the contact surface (BP10_3).

Bent connectors were removed from damaged models, inspected and their permanent deformation was evaluated—see Figure 8. The shape of connectors was originally flat in areas of anchoring in joints. However, permanent deformation occurred in the central area where connectors crossed the wall joints. A permanent displacement u_u perpendicular to the flat connector axis was observed in the section marked e_u . Additionally, the representative total extension of each connector δ_u was calculated. A permanent displacement e_u in models B10 ranged from 20 mm to 27 mm, and the mean was 23 mm (23t) at the mean displacement u_u between 8 mm and 17 mm and a mean of 11 mm (11t). A permanent displacement e_u in models BP10 ranged from 20 mm to 29 mm, and the mean was 23 mm (23t). The vertical displacement u_u was between 8 mm and 17 mm, and the mean was 12 mm (12t). Deformation seemed to be identical despite the shape of the connectors. The only reported difference was the position of the deformed area regarding the mid-length of the connector. Displacements observed for some connectors were of the order of ± 20 mm with respect to the mid-length of the connector. As no regularity caused by, e.g., their position in joints was found, the above was assumed to be the effect of precisely made joints. The measured geometry of the connectors in each model and the mean values are presented in Table 8.

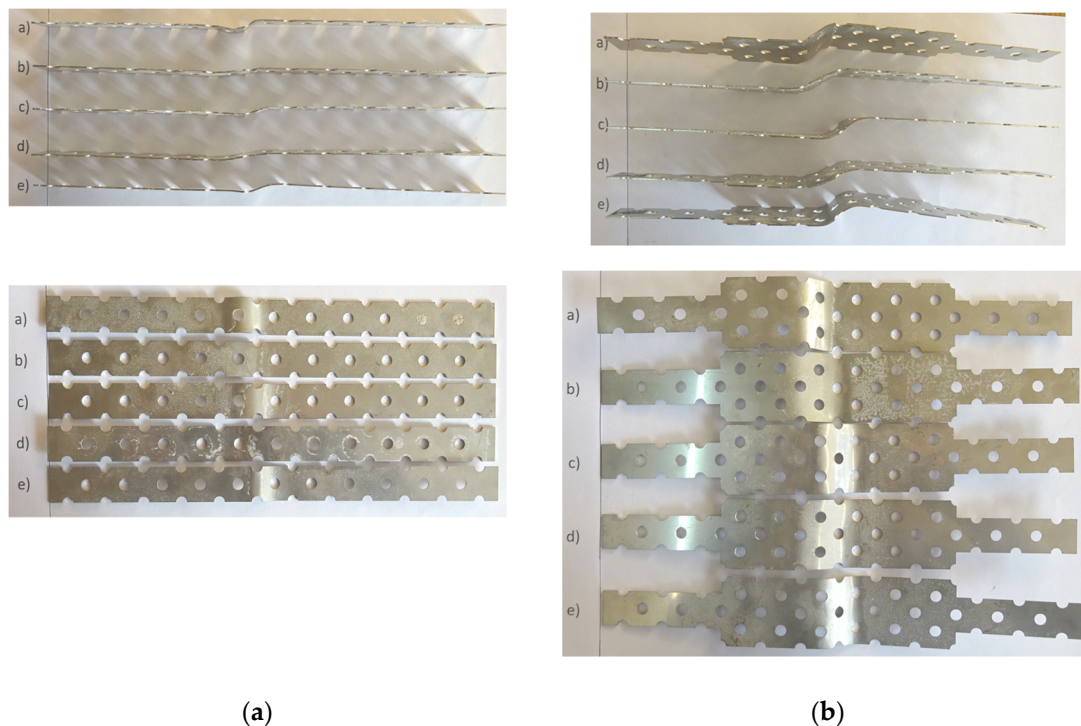


Figure 8. Deformed connectors removed from damaged test models after tests: (a) punched flat profiles in the wall B10_2, (b) punched widened flat profiles in the wall BP10_2.

Table 8. Measured geometry of deformed connectors.

| Model | | Layer of Connectors | | | | | |
|--------|---|---------------------|-------------|--|-------------|---|-----------------|
| | | | | Distance between Points of Contraflexure | | Relative Displacement of Connector Ends | |
| | | | | $e_{u,i}$ | $e_{u,mv}$ | $u_{u,i}$ | $u_{u,mv}$ |
| | | | | $\delta_{u,i} = \sqrt{e_u^2 + u_u^2} - e_{u,mv}$ | | | |
| | | | | mm | mm | mm | mm |
| 1 | 2 | 3 | 4 | 5 | 6 | 7 | 8 |
| B10_1 | a | 23 | | 9 | | 1.70 | |
| | b | 21 | | 8 | | 1.47 | |
| | c | 20 | 22 | 9 | 9 | 1.93 | 1.8 |
| | d | 24 | | 9 | | 1.63 | |
| | d | 21 | | 10 | | 2.26 | |
| B10_2 | a | 26 | | 11 | | 2.23 | |
| | b | 26 | | 10 | | 1.86 | |
| | c | 25 | 24 | 11 | 10 | 2.31 | 2.2 |
| | d | 22 | | 10 | | 2.17 | |
| | d | 20 | | 10 | | 2.36 | |
| B10_3 | a | 21 | | 11 | | 2.71 | |
| | b | 23 | | 13 | | 3.42 | |
| | c | 23 | 23 | 15 | 14 | 4.46 | 3.7 |
| | d | 23 | | 12 | | 2.94 | |
| | d | 27 | | 17 | | 4.91 | |
| | | | 23 (23t) | – | 11 (11t) | – | 2.57 (2.57t) |
| BP10_1 | a | 19 | | 12 | | 3.47 | |
| | b | 27 | | 14 | | 3.41 | |
| | c | 24 | 24 | 13 | 13 | 3.29 | 3.33 |
| | d | 29 | | 11 | | 2.02 | |
| | d | 23 | | 15 | | 4.46 | |
| BP10_2 | a | 23 | | 17 | | 5.60 | |
| | b | 22 | | 14 | | 4.08 | |
| | c | 27 | 23 | 14 | 15 | 3.41 | 4.22 |
| | d | 22 | | 13 | | 3.55 | |
| | d | 23 | | 15 | | 4.46 | |

Table 8. Cont.

| 1 | 2 | 3 | 4 | 5 | 6 | 7 | 8 |
|--------|---|----|-------------|----|-------------|------|-----------------|
| BP10_3 | a | 22 | | 12 | | 3.06 | |
| | b | 23 | | 10 | | 2.08 | |
| | c | 19 | 23 | 9 | 10 | 2.02 | 2.01 |
| | d | 26 | | 8 | | 1.20 | |
| | d | 23 | | 9 | | 1.70 | |
| | | | 23 (23t) | – | 13 (13t) | – | 3.28 (2.57t) |

As the in case of unreinforced joints, phases of reinforced joints can be presented in diagrams illustrating the relationship between the load N and relative (mutual) displacement u of joined walls—see Figure 9.

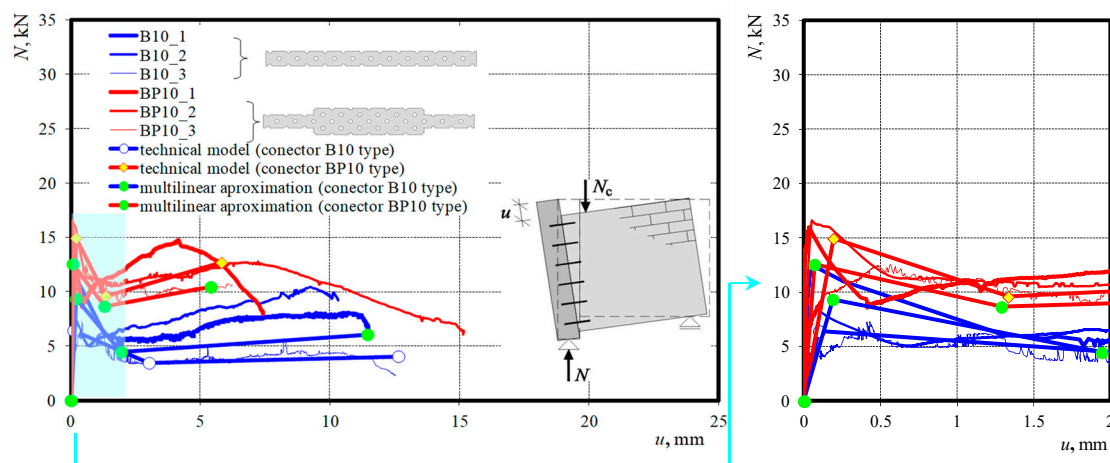


Figure 9. Relationship between the total force and mean displacement of joints.

Until the crack on the contact area that appeared under the maximum load $N_{cr} = N_u = 7.3\text{--}12.3$ kN for models **B10** and $12.5\text{--}16.5$ kN for models **BP10**, an increment in displacement was nearly proportional and that phase was defined as the elastic phase. A clear increase in displacements and a drop in force to $N_d = 3.4\text{--}5.0$ kN in models **B10** and $8.9\text{--}10.5$ kN in models **BP10** was observed after cracking in the failure phase. When the force N_d was reached in the failure phase, the joint demonstrated the capacity to take load, and a small hardening was noticed. The failure of the models caused by excessive displacements was observed under the maximum load $N_{cr} = N_u = 2.3\text{--}9.2$ kN for models **B10** and $10.6\text{--}14.8$ kN for models **BP10**. Thus, a drop in the residual force of the maximum force was ca. 35% for models **B10** and only 15% for models **BP10**. Connectors **B10** produced lower values of the force in individual phases. Loading at the time of cracking was lower by 76%, and the maximum loading was lower by as much as 82%. Moreover, the residual force was lower by 63% when compared to the force determined for unreinforced models. Displacements in the reinforced models at the greatest force were lower only by 18% compared to the unreinforced joint. Displacements in reinforced joints greater than 100% were found under the residual force at the end of the failure phase. When compared to the unreinforced models, the cracking force acting on the models with connectors **BP10** with a widened central part was lower by 62% than in the model with the traditional joint. The maximum cracking force acting on the reinforced models was lower by 71% than in the case of the unreinforced models. Furthermore, the residual force was greater by more than 63%. Displacements in the reinforced models at the greatest force were lower by 15% than in the unreinforced joint. Moreover, displacements slightly greater by 4% than in unreinforced models were observed under the residual force at the end of

the failure phase. A twofold widening of the connector in the models **BP10** resulted in ca. 60% increase in forces N_u and over 100% increase in forces N_d and N_r when compared to results obtained for models **B10**. Displacements in the models with wider connectors were as expected—almost identical in the elastic phase and lower by 30%–50% in the failure phase. The observed phases were the basis of a multi-linear diagram illustrating the N – u relationship for joints in AAC walls—see Figure 10. The elastic phase was defined within the loading range 0 – $N_{cr} = N_u$, and the failure phase within the range N_u – N_d – N_r .

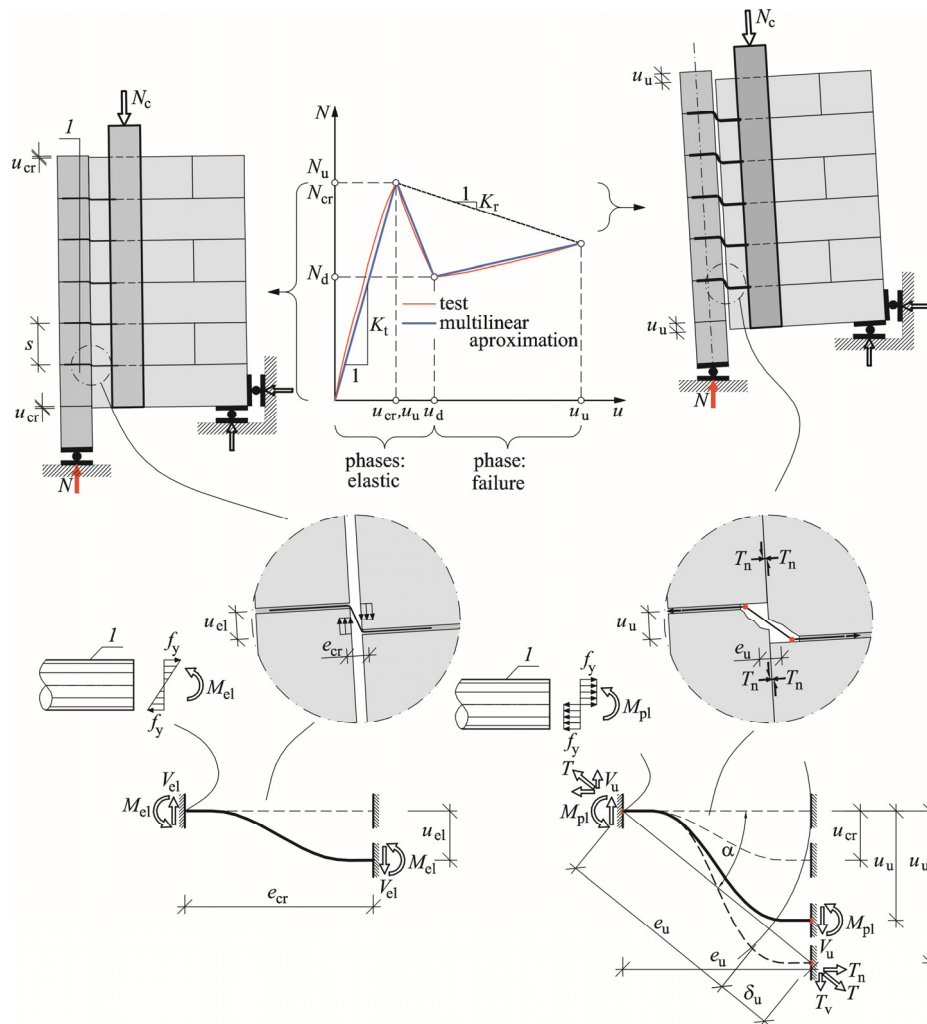


Figure 10. Approximation of work of reinforced joint between masonry walls (connector (1)).

Values of forces and corresponding displacements are presented in Tables 9 and 10. Joint stiffnesses were determined in each phase according to Equations (1)–(3) and they are presented in Table 11. A linear approximation of results is shown in Figure 10.

Table 9. Test results for reinforced joints (forces).

| Model | Cracking Force | | Force at Failure | | Dowel Force | | Residual Force | |
|--------|------------------|-------------------|------------------|------------------|-------------|--------------------|-----------------|------------------|
| | $N_{cr,i}$ kN | $N_{cr,mv}$ kN | $N_{u,i}$ kN | $N_{u,mv}$ kN | N_d kN | $N_{d,mv,i}$ kN | $N_{r,i}$ kN | $N_{r,mv}$ kN |
| B10_1 | 12.3 | | 12.3 | | 5.01 | | 6.68 | |
| B10_2 | 8.41 | 9.3 | 8.41 | 9.3 | 5.02 | 4.5 | 9.20 | 6.1 |
| B10_3 | 7.27 | | 7.27 | | 3.39 | | 2.32 | |
| BP10_1 | 15.9 | | 15.9 | | 8.86 | | 14.8 | |
| BP10_2 | 16.5 | 14.9 | 16.5 | 14.9 | 10.5 | 9.6 | 12.6 | 12.7 |
| BP10_3 | 12.4 | | 12.4 | | 9.36 | | 10.6 | |

Table 10. Test results for reinforced joints (displacements).

| Model | Displacement at the Time of Cracking | | Displacement Right before Failure | | Displacement at Dowel Force | | Residual Displacement | |
|--------|--------------------------------------|-------------------|-----------------------------------|------------------|-----------------------------|------------------|-----------------------|------------------|
| | $u_{cr,i}$ mm | $u_{cr,mv}$ mm | $u_{u,i}$ mm | $u_{u,mv}$ mm | $u_{d,i}$ mm | $u_{d,mv}$ mm | $u_{r,i}$ mm | $u_{r,mv}$ mm |
| B10_1 | 0.07 | | 0.07 | | 1.83 | | 11.50 | |
| B10_2 | 0.08 | 0.19 | 0.08 | 0.19 | 0.68 | 1.94 | 10.33 | 11.45 |
| B10_3 | 0.41 | | 0.41 | | 3.32 | | 12.52 | |
| BP10_1 | 0.04 | | 0.04 | | 0.45 | | 4.15 | |
| BP10_2 | 0.05 | 0.19 | 0.05 | 0.19 | 1.61 | 1.33 | 7.04 | 5.80 |
| BP10_3 | 0.49 | | 0.49 | | 1.94 | | 6.22 | |

Table 11. Test results for reinforced joints (stiffness).

| Model | Elastic Joint Stiffness | | Residual Joint Stiffness | |
|--------|-------------------------|--------------------|--------------------------|--------------------|
| | $K_{t,i}$ MN/m | $K_{t,mv}$ MN/m | $K_{r,i}$ MN/m | $K_{r,mv}$ MN/m |
| B10_1 | 180 | | 0.496 | |
| B10_2 | 102 | 100 | 0.077 | 0.327 |
| B10_3 | 17.8 | | 0.409 | |
| BP10_1 | 432 | | 0.269 | |
| BP10_2 | 319 | 259 | 0.553 | 0.378 |
| BP10_3 | 25.6 | | 0.312 | |

Validation of the Model Representing Reinforced Joints in Walls

Like for unreinforced joints, the obtained results were generalised. The following assumptions were made:

- d) A non-linear relationship $N-u$ determined from tests was replaced with a multi-linear relationship expressing all observed phases:
 - i. the elastic phase observed in the load range $0 - N_{cr} = N_u$;
 - ii. the failure phase observed in the load range $N_u - N_d - N_r$.
- e) It was suggested that all material parameters used in the model should be specified using standard and normalised methods;

- f) An elastic and perfectly plastic model of the connector was used;
- g) The model would be subjected to statistical validation on the basis of performed tests.

The behaviour of the joint was described with simplified solutions found in the literature [20,21]. According to the cited papers, connectors were working as bars fixed on both sides, and the value of the force causing the displacement u could be expressed as follows:

$$V = \frac{12E_s I}{e^3} u, \quad (13)$$

the corresponding bending moment in the connector is equal to:

$$M = \frac{6E_s I}{e^2} u, \quad (14)$$

where EI is the flexural stiffness of the connector, u is the relative displacement of the connector ends and e is the representative length of the connector (distance between points of contraflexure).

Stress values of extreme fibres in the connector fixed in bed joints increased proportionally to the displacement u . For some displacements u_{el} , stress at extreme fibres reached the yield point, and the bending moment and the shearing force were expressed via the following equations:

$$M_{el} = f_y W_{el} = \frac{6E_s I}{e_{el}^2} u_{el}, \quad V_{el} = \frac{2M_{el}}{e_{el}}. \quad (15)$$

where W_{el} is the elastic indicator of the transverse bending of the connector section, f_y is the representative yield point of steel in the connector and e_{el} is the connector length in the elastic phase.

An increase in the relative displacements of the ends of connectors was observed with the yielding of the total section of the connector, resulting in the highest bending moment and the greatest shearing force equal to:

$$M_{pl} = f_y W_{pl} = \frac{6E_s I}{e_{pl}^2} u_{pl}, \quad V_u = \frac{2M_{pl}}{e_{pl}}, \quad (16)$$

where W_{pl} is the plastic index of the transverse bending of the connector section, f_y is the representative yield point of steel in the connector and e_{pl} is the connector length in the plastic phase.

An increase in relative displacements could cause the spalling of the wall beneath the connector and an increase in the length of connectors. This, in turn, could produce a noticeable drop in the force in the joints. As in previous phases, bending moments in connectors and shearing forces were determined from the following relationship:

$$M_d = f_y W_{pl} = \frac{6E_s I}{e_d^2} u_d, \quad V_d = \frac{2M_d}{e_d}, \quad (17)$$

Tests demonstrated that a further increase in relative displacements could cause an increase in the forces in joints. In that phase, displacements were so considerable that connectors could work in a flexible and also a tendon mode. Consequently, friction force was generated between the joined walls. The bending moment and shearing forces in the joint can be expressed as:

$$M_u = f_y W_{pl} = \frac{6E_s I}{e_u^2} u_u, \quad V_u = \frac{2M_u}{e_u}, \quad (18)$$

And the axial force in the joint induced by tendon work was:

$$T = E_s A \frac{\delta_u}{e_u}, \quad (19)$$

where δ_u is the extension of the connector, determined from the following equation:

$$\delta_u = \sqrt{e_u^2 + u_u^2} - e_u. \quad (20)$$

The horizontal and vertical components of force, being the effects of the tendon work (at $\alpha \approx 0$), were equal to:

$$\begin{aligned} T_h &= T \cos \alpha \approx T, \\ T_v &= T \sin \alpha \approx 0. \end{aligned} \quad (21)$$

Taking into account the tendon work of connectors, the load capacity of reinforced joints in walls can be expressed as:

$$V_u = \frac{2f_y W_{pl}}{e_u} n_c + \alpha n_c E_s A \frac{\delta_u}{e_u} \mu, \quad (22)$$

where μ is the friction coefficient α is the empirical coefficient, e_u is the average length of the connector (distance between points of contraflexure acc. to Table 8) and $n_c = 5$ is the number of connectors.

The corresponding displacement is expressed by the following relationship:

$$u_u = \frac{f_y W_{pl} e_u^2}{6E_s I} \beta, \quad (23)$$

where μ is the friction coefficient and β is the empirical coefficient.

Forces in the failure phase can be determined similarly.

$$V_d = \frac{2f_y W_{pl}}{e_u} n_c + \alpha_1 n_c E_s A \frac{\delta_u}{e_u} \mu, \quad (24)$$

$$u_d = \frac{f_y W_{pl} e_u^2}{6E_s I} \beta_1, \quad (25)$$

$$V_r = \frac{2f_y W_{pl}}{e_u} n_c + \alpha_2 n_c E_s A \frac{\delta_u}{e_u} \mu, \quad (26)$$

$$u_r = \frac{f_y W_{pl} e_u^2}{6E_s I} \beta_2. \quad (27)$$

Above equations included not only the mechanical parameters of the connectors (E, f_y) but also the measured length of connectors e_u —the distance between points of contraflexure. However, this approach is not unconditional. The length of connectors measured in the tests was ca. $23t$. The authors in [20] determined experimentally that the length of connectors from flat profiles was $(1.6\text{--}2.5)t$, provided that masonry units below the connector were not crushed as observed in the models made of AAC. Like for unreinforced models, the values of empirical coefficients were calculated using results from material tests and tests on individual elements. Boundary values of mean coefficients $\alpha, \alpha_1, \alpha_2, \beta, \beta_1, \beta_2$ were determined at the significance level $\alpha = 0.8$. As the sample size was small, the relationship expressed by the relationship in Equation (11) was used. Lower and upper values from the confidence interval of mean coefficients are presented in Table 12.

Table 12. Validation of empirical coefficients of the model with reinforced wall joints.

| Model | x_i | | | | | |
|---|---|---|--|--|--|--|
| | $\alpha_i = \frac{V_{u,i} - \frac{2f_y W_{pl}}{e_u} n_c}{n_c E_s A \frac{\delta_u}{e_u} \mu}$ | $\beta_i = \frac{6E_s I u_{u,i}}{f_y W_{pl} e_u^2}$ | $\alpha_{1i} = \frac{V_{d,i} - \frac{2f_y W_{pl}}{e_u} n_c}{n_c E_s A \frac{\delta_u}{e_u} \mu}$ | $\beta_{1i} = \frac{6E_s I u_{d,i}}{f_y W_{pl} e_u^2}$ | $\alpha_{2i} = \frac{V_{r,i} - \frac{2f_y W_{pl}}{e_u} n_c}{n_c E_s A \frac{\delta_u}{e_u} \mu}$ | $\beta_{2i} = \frac{6E_s I u_{r,i}}{f_y W_{pl} e_u^2}$ |
| B10_1 | 0.01117 | 0.10 | 0.00421 | 2.73 | 0.00580 | 17.2 |
| B10_2 | 0.00744 | 0.12 | 0.00422 | 1.02 | 0.00819 | 15.4 |
| B10_3 | 0.00636 | – | 0.00268 | – | – | 18.7 |
| n | 3 | 2 | 3 | 2 | 2 | 3 |
| \bar{x} | 0.00832 | 0.11 | 0.003702 | 1.88 | 0.00699 | 17.11 |
| S | 0.00253 | 0.0146 | 0.0008880 | 1.21 | 0.00169 | 1.63 |
| $t_{1-\alpha/2}$ | 1.89 | 3.08 | 1.89 | 3.08 | 3.08 | 1.89 |
| $\bar{x} - t_{1-\alpha/2} \frac{S}{\sqrt{n}}$ | 0.00557 | 0.081 | 0.00274 | −0.75 | 0.0033 | 15.33 |
| $\bar{x} + t_{1-\alpha/2} \frac{S}{\sqrt{n}}$ | 0.01107 | 0.145 | 0.00467 | 4.50 | 0.0107 | 18.89 |
| BP10_1 | 0.00619 | 0.06 | 0.00328 | | 0.00573 | |
| BP10_2 | 0.00645 | 0.08 | 0.00397 | 2.43 | 0.00484 | 10.6 |
| BP10_3 | 0.00476 | | 0.00348 | 2.91 | 0.00401 | 9.4 |
| n | 3 | 2 | 3 | 2 | 3 | 2 |
| \bar{x} | 0.00580 | 0.07 | 0.00358 | 2.67 | 0.00486 | 9.98 |
| S | 0.000911 | 0.0 | 0.000356 | 0.3 | 0.000859 | 0.877 |
| $t_{1-\alpha/2}$ | 1.89 | 3.08 | 1.89 | 3.08 | 1.89 | 3.08 |
| $\bar{x} - t_{1-\alpha/2} \frac{S}{\sqrt{n}}$ | 0.0048 | 0.0319 | 0.00319 | 1.93 | 0.0039 | 8.1 |
| $\bar{x} + t_{1-\alpha/2} \frac{S}{\sqrt{n}}$ | 0.0068 | 0.1014 | 0.0040 | 3.41 | 0.0058 | 11.9 |

Following the procedure conducted for unreinforced joints, two values defining lower and upper limits of confidence intervals matched each of the six coefficients (Table 12). Thus, there were $\binom{6}{2}$ different combinations (without any repetitions) for coefficients. Similarly, as for unreinforced joints, the minimum value of the mean percentage error (MPE) [19] was applied as a selection criterion separately for forces and displacements. Optimal values of those coefficients were calculated from 15 combinations. For the values of coefficients in the shaded cells in Table 12, the minimum MPE for forces and displacements in connectors B10 was equal to 22%. For connectors BP10, the MPE for forces and displacements was 11%. Using results from the model and standard tests, empirical relationships describing the work of joints in particular phases are presented in Table 13, and calculated values and empirically obtained values are compared in Table 14 and Figure 10.

Table 13. Relationships expressing the work of reinforced joints in walls.

| Joint Phase | Force | Stiffness | Displacement |
|----------------|---|-----------------------------------|--|
| Connector B10 | | | |
| Elastic phase | $V_u = \frac{2f_y W_{pl}}{e_u} n_c + 0.0056 c E_s A \frac{\delta_u}{e_u} \mu$ | $K_t = V_u / u_u$ | $u_u = 0.145 \frac{f_y W_{pl} e_u^2}{6 E_s I}$ |
| Failure phase | $V_d = \frac{2f_y W_{pl}}{e_u} n_c + 0.0027 n_c E_s A \frac{\delta_u}{e_u} \mu$ | $K_r = (V_u - V_r) / (u_r - u_u)$ | $u_d = 4.50 \frac{f_y W_{pl} e_u^2}{6 E_s I}$ |
| | $V_r = \frac{2f_y W_{pl}}{e_u} n_c + 0.0023 n_c E_s A \frac{\delta_u}{e_u} \mu$ | | $u_r = 18.9 \frac{f_y W_{pl} e_u^2}{6 E_s I}$ |
| Connector BP10 | | | |
| Elastic phase | $V_u = \frac{2f_y W_{pl}}{e_u} n_c + 0.0048 n_c E_s A \frac{\delta_u}{e_u} \mu$ | $K_t = V_u / u_u$ | $u_u = 0.10 \frac{f_y W_{pl} e_u^2}{6 E_s I}$ |
| Failure phase | $V_d = \frac{2f_y W_{pl}}{e_u} n_c + 0.0032 n_c E_s A \frac{\delta_u}{e_u} \mu$ | $K_r = (V_u - V_r) / (u_r - u_u)$ | $u_d = 1.93 \frac{f_y W_{pl} e_u^2}{6 E_s I}$ |
| | $V_r = \frac{2f_y W_{pl}}{e_u} n_c + 0.0039 n_c E_s A \frac{\delta_u}{e_u} \mu$ | | $u_r = 8.1 \frac{f_y W_{pl} e_u^2}{6 E_s I}$ |

Table 14. Compared tests results and own calculations for the standard model.

| Test results for connector B10 | | | Calculations for connector B10 | | |
|---------------------------------|-------------------|------------------|--|-------------------|-------------------|
| forces | | | forces | | |
| $N_{cr,mv} = N_{u,mv}$ kN | $N_{d,mv}$ kN | $N_{r,mv}$ kN | $N_{cr,cal} = N_{u,cal}$ kN | $N_{d,cal}$ kN | $N_{r,cal}$ kN |
| 9.34 | 4.47 | 6.07 | 6.44 | 3.45 | 4.06 |
| Displacements of connector B10 | | | Calculated displacements of connector B10 | | |
| $u_{cr,mv} = u_{u,mv}$ mm | $u_{ag,mv}$ mm | $u_{r,mv}$ mm | $u_{cr,cal} = u_{u,cal}$ mm | $u_{u,cal}$ mm | $u_{r,cal}$ mm |
| 0.19 | 1.94 | 11.45 | 0.10 | 3.01 | 12.6 |
| Test results for connector BP10 | | | Calculations for connector BP10 | | |
| force | | | force | | |
| $N_{cr,mv} = N_{u,mv}$ kN | $N_{d,mv}$ kN | $N_{r,mv}$ kN | $N_{cr,cal} = N_{u,cal}$ kN | $N_{d,cal}$ kN | $N_{r,cal}$ kN |
| 14.94 | 9.59 | 12.69 | 12.6 | 8.65 | 10.43 |
| Displacements of connector BP10 | | | Calculated displacements of connector BP10 | | |
| $u_{cr,mv} = u_{u,mv}$ mm | $u_{ag,mv}$ mm | $u_{r,mv}$ mm | $u_{cr,cal} = u_{u,cal}$ mm | $u_{u,cal}$ mm | $u_{r,cal}$ mm |
| 0.19 | 1.33 | 5.80 | 0.07 | 1.29 | 5.40 |

For standard connectors **B10** without widening, calculated forces determining coordinates of particular phases were lower than those obtained during tests. The difference for the maximum force was equal to 31%, and for the aggregate interlocking force –23%. The value of the force N_r in the failure phase was lower by 33% than the empirical value. Similar results were obtained for connectors **BP10**. Determined force values were lower than experimental ones. The maximum force N_u was lower by 16%, and forces V_d and V_r in the failure phase were lower by 10% and 18%, respectively, when compared to forces determined experimentally. Calculated displacements of joints with connectors **B10** varied significantly. The calculated displacement at failure was lower by 48% than the experimentally determined values. Moreover, displacements in the failure phase corresponding to the force V_d were greater by over 55% than experimental values, and calculated displacements were greater only by 10%. For connectors **BP10**, displacements at the maximum force were underestimated at a level of

over 65%, and overestimated by only 3% under the force V_d . Differences in calculated and measured displacements at failure were equal to just 7%.

The obtained results, particularly for forces, can be used to estimate, with safe margins, the forces in joints and to verify SLS conditions where no guidelines can be applied. As for unreinforced joints, the greatest differences were observed for displacements. The recommended relationships can cause a significant underestimation of displacement at failure, even at the level of ca. 50%.

4. Conclusions

Tests described in this paper are a part of a piece of complex research work conducted at the Silesian University of Technology. This paper presents results from testing three types of wall joints: a traditional mortar bonding (URM), joints with punched steel flat profiles (**B10**) and with connectors of genuine shape (**BP10**) protected by the patent.

The failure process and crack development on the walls bonded with mortar were mild and included three phases. Distinct wall cracks near the joint were observed prior to failure. Failure and cracking of models with steel elements, apart from lower load capacity, were completely different. No cracks preceding the wall destruction were observed, but there were rapid displacements and a drop in loading. For perforated flat profiles used as steel connectors, significantly lower values were obtained when compared to the models with mortar bonding. Forces at the time of cracking were lower by 62% (**BP10**) and 76% (**B10**), and the difference at the maximum force was 82% (**BP10**) and 71% (**B10**). Reinforced models were less deformed in the elastic phase. Differences at the maximum force were 18% (**B10**) and 15% (**BP10**). Greater differences were observed for displacements prior to the failure. Displacements in the models with reinforced joints **B10** were greater by over 100% than in unreinforced models. Generally, the same displacements were reported for the models with connectors **BP10**. A twofold widening of the connector in models **BP10** resulted in a ca. 60% increase in maximum forces when compared to results obtained for models **B10**. Displacements in the models with wider connectors were as expected and almost identical in the elastic phase and lower by 30%–50% in the failure phase.

Particular phases of joint work were determined and defined, and an empirical approach was proposed to determine the forces and displacement of wall joints using the results from less complicated standard tests. Values of cracking and failure forces were estimated with a safety margin for unreinforced joints. Moreover, they differed by 15% and 9% in comparison to the test results. On the basis of relationships described in the literature [20,21], a technical solution was proposed, which included the determination of forces producing cracks on the contact area and maximum forces in joints between walls reinforced with punched flat profiles. Due to the small number of elements per series, differences in the safe estimation of forces were of the order of 31% for maximum forces in connector **B10**, and 26% in connector **BP10**.

Work should be continued and additional test models should be constructed to define the statistically empirical parameters of models. Then, the results of validation can be expected to provide lower differences in extreme values. Moreover, FEM (Finite Element Method)-based analyses seem to be necessary to determine the real work of joints, particularly to determine their real length (e). The target model should also give consideration to the phase of joint weakening and to the estimation of forces N_{cr} , N_d and N_u and corresponding displacements with satisfactory accuracy.

Author Contributions: Conceptualization, R.J. and I.G.; methodology, R.J. and I.G.; validation, R.J.; formal analysis, I.G.; investigation, I.G.; writing—original draft preparation, R.J.; writing—review and editing, I.G.; visualization, R.J. and I.G.; supervision, R.J. and I.G. All authors have read and agreed to the published version of the manuscript.

Funding: The research was financed from the own funds of the Department of Building Structures and Department of Structural Engineering Silesian University of Technology and project: NB-323/RB-2/2017 Experimental tests of joints in masonry walls made of autoclaved aerated concrete, financed by Solbet Company.

Acknowledgments: The authors would like to express particular thanks to Solbet and NOVA companies for valuable suggestions and the delivery of masonry units, mortar, and connectors which were used to prepare test models and perform tests.

Conflicts of Interest: The authors declare no conflict of interest.

References

1. Castro, L.O.; Alvarenga, R.D.C.S.; Silva, R.M.; Ribeiro, J.C.L. Experimental evaluation of the interaction between strength concrete block walls under vertical loads. *Revista Ibracon de Estruturas e Materiais* **2016**, *9*, 643–681. [\[CrossRef\]](#)
2. Paganoni, S.; D’Ayala, D. Testing and design procedure for corner connections of masonry heritage buildings strengthened by metallic grouted anchors. *Eng. Struct.* **2014**, *70*, 278–293. [\[CrossRef\]](#)
3. Maddaloni, G.; Balsamo, A.; Di Ludovico, M.; Prota, A. Out of Plane Experimental Behavior of T-Shaped Full Scale Masonry Orthogonal Walls Strengthened with Innovative Composite Systems. In Proceedings of the Fourth International Conference on Sustainable Construction Materials and Technologies, Las Vegas, NV, USA, 7–11 August 2016.
4. Maddaloni, G.; Di Ludovico, M.; Balsamo, A.; Prota, A. Out-of-plane experimental behaviour of T-shaped full scale masonry wall strengthened with composite connections. *Compos. Part B Eng.* **2016**, *93*, 328–343. [\[CrossRef\]](#)
5. Galman, I.; Jasiński, R.; Hahn, T.; Konopka, K. Study of joints masonry walls. *Materiały Budowlane* **2017**, *10*, 94–96. (In Polish) [\[CrossRef\]](#)
6. Galman, I.; Jasiński, R. Joints in masonry walls. *Ce/papers* **2018**, *2*, 339–346. [\[CrossRef\]](#)
7. Galman, I.; Jasiński, R. Tests of joints in AAC masonry walls. *Arch. Civ. Eng. Environ.* **2018**, *11*, 79–92. [\[CrossRef\]](#)
8. Polish Patent Office. Wall Joint Connector. Niepodległości 188/192, 00-950 Warsaw (Poland). Patent No. W.128,153, 1 April 2019.
9. PN-EN 1052-1:2000 Methods of Tests for Masonry. *Part 1: Determination of Compression Strength*; Polish Committee for Standardization (PKN): Warsaw, Poland, 2000. (In Polish)
10. Jasiński, R.; Drobiec, Ł. Comparison Research of Bed Joints Construction and Bed Joints Reinforcement on Shear Parameters of AAC Masonry Walls. *J. Civ. Eng. Arch.* **2016**, *10*, 1329. [\[CrossRef\]](#)
11. PN-EN 1052-3:2004 Methods of Tests for Masonry. *Part 3: Determination of Initial Shear Strength*; Polish Committee for Standardization (PKN): Warsaw, Poland, 2004. (In Polish)
12. Drobiec, Ł.; Jasiński, R. Influence of the kind of mortar on mechanical parameters of AAC masonry subjected to shear – the basic strength parameters. *Materiały Budowlane* **2015**, *5*, 106–109. (In Polish) [\[CrossRef\]](#)
13. Jasiński, R. Research and Modelling of Masonry Shear. Walls. Thesis, Silesian University of Technology, Gliwice, Poland, 2017.
14. ASTM E519-81. *Standard Test Method for Diagonal Tension (Shear) of Masonry Assemblages*; American Society for Testing and Materials: West Conshohocken, PA, USA, 2000.
15. Drobiec, Ł.; Jasiński, R. Influence of the kind of mortar on mechanical parameters of AAC masonry subjected to shear—dilatational deformability. *Materiały Budowlane* **2015**, *7*, 116–119. (In Polish) [\[CrossRef\]](#)
16. PN-EN 10002-1:2004 Metallic Materials—Tensile Testing. *Part 1. Method of Test at Ambient Temperature*; Polish Committee for Standardization (PKN): Warsaw, Poland, 2004. (In Polish)
17. Galman, I.; Jasiński, R. Attempt to Describe the Mechanism of Work of Masonry Joints. *IOP Conf. Series Mater. Sci. Eng.* **2019**, *471*, 052054. [\[CrossRef\]](#)
18. Volk, W. *Applied Statistics for Engineers*; Literary Licensing, LLC: Whitefish, MT, USA, 2013.
19. David, F.; Robert, P.; Roger, P. *Statistics*, 4th ed.; W.W. Norton & Company: New York, NY, USA, 2007.

20. Simudic, G.; Page, A.W. Australian Developments in the Use of Walls of Geometric Section. In Proceedings of the 7th North American Masonry Conference, University of Notre Dame-South Bend, South Bend, IN, USA, 2–5 June 1996; Volume 2, pp. 1007–1018.
21. Phipps, M.E.; Montague, T.I. The Behaviour and Design of Steel Shear Connectors in Plain and Prestressed Masonry. In Proceedings of the 7th North American Masonry Conference, University of Notre Dame-South Bend, South Bend, IN, USA, 2–5 June 1996; Volume 2, pp. 789–798.



© 2020 by the authors. Licensee MDPI, Basel, Switzerland. This article is an open access article distributed under the terms and conditions of the Creative Commons Attribution (CC BY) license (<http://creativecommons.org/licenses/by/4.0/>).